

DEVELOPMENT AND EVALUATION OF A VTOL OBSERVATION PLATFORM

Moad Yacoubi^Ψ, Simon Delpire^Ψ, Ibrahim Idlbi^Υ and Patrick Hendrick^Ψ

^Ψ *Aero-Thermo-Mechanics Department, Université Libre de Bruxelles,
50, F.D. Roosevelt Avenue, 1050 Brussels - Belgium,*

^Υ *Concordia University (Canada),*

1455 De Maisonneuve Blvd. W., Montreal, QC H3G 1M8 - Canada

^Γ *Aerospace and Mechanical Engineering Department, University of Liège*

1, Chemin des Chevreuils, 4000 Liège - Belgium

myacoubi@ulb.ac.be

Abstract

Within the context of the latest Minidrones competition held by the French Aerospace Lab ONERA, the Université Libre de Bruxelles (ULB) is continuing the development and optimization of a ducted rotor MAV, that was specifically developed for this competition and for which Vertical Take-off and Landing (VTOL) capabilities and autonomous flight were mandatory.

In this paper we present some experimental results obtained with this ducted rotor UAV. A detailed analysis of the validity of the tests and their reproducibility is presented. We discuss the tests that have been retained in order to draw some conclusions. Finally we briefly present a method for calculating the volume of the hydrogen necessary for fueling a fuel cell that would be integrated into the UAV in order to increase its autonomy.

1 INTRODUCTION



FIGURE 1 – The ducted fan MAV of ULB

The Unmanned Aerial Vehicles (UAVs) exist in various sizes. One of the most interesting niches concerns the UAVs of moderate size ($< 1m$), also called Micro Air Vehicles (MAVs). An aerodynamic study of the ULB-developed ducted rotor MAV (Figure 1) using the results of full-scale wind tunnel tests allowed the determination of the platform's flight speed envelope, power requirements and endurance characteristics for ISA sea level conditions.

Vertical Take-off and Landing (VTOL) UAVs have many advantages, including hovering, flying at low speeds, vertical takeoff and active movement capability.

There are different types of VTOL MAV featuring different mechanical designs, number of rotors etc. Naturally, more rotors will require more power to operate while less rotors will require less power to operate, but this statement may not be necessarily true if an appropriate modeling and control strategy is employed[4].

Comparing some types of multi rotor UAV, we see that the Quadri-rotor UAV has some advantages, which include simplified rotor mechanics, increased payload and reduced gyroscopic effects. The disadvantages of such UAVs may include an increase weight and a high energy consumption[9]. The six-rotor UAV is very stable and can be compressed by using two layers of three rotors, but its disadvantages include high energy consumption[5]. The main advantage of the eight-rotor UAV is that its attitude dynamics is decoupled from the translation dynamics[1].

Nevertheless, all these solutions are limited in payload and autonomy due to their high energy consumption. The contra-rotating (or counter-rotating) co-axial rotors UAV appears very interesting because it offers better performance in stationary flight and completely eliminates yaw stabilization problems. However, this limit the directional maneuverability of the aircraft and degrades horizontal flight performance. In addition, the two rotors must be placed at a safe distance to prevent any contact between their blades, thus increasing the height of the UAV.

It follows that there is no optimal design solution for MAVs. Nevertheless, from a weight minimization point of view, the single ducted fan concept is quite promising. The ULB's ducted rotor MAV (Figure 2) features two stages of control vanes in the wake of the rotor. The role of the vanes is to stabilize the aircraft and to control low speed flight.

The duct increases the aerodynamic efficiency of the rotor and protects users from the high-speed blade tips. The UAV can be handled without any risk when in hover mode.

The ratio between the duct outlet's area and rotor area is greater than one, i.e. the duct is diverging. This divergence limits the contraction of the air tube at the exit of the rotor and thus increases the available thrust. Also, the proximity of the blade tip to the fairing eliminates edge effects and therefore reduces tip losses.

Yaw control is achieved by the first stage of control vanes (Figure 2), named stator, and composed of four variable camber blades of which the primary function is the compensation of motor torque. These "anti-torque" blades are installed in the duct at a predetermined angle with respect to the vertical axis of symmetry, producing a lift force and thus torque commensurate with the rotor's rotational speed Ω_r . This setup allows the use of a single rotor without having to make excessive control corrections. Furthermore, it separates the yaw control from the roll and pitch control.

Roll and pitch control is provided by the second stage (Figure 2), a set of four pairs of blades installed below the anti-torque blades. Two pairs of blades control the MAV in pitch. The other two pairs provide roll control. The angle of attack of the blades is controlled by servomotors installed in the center fuselage. This configuration eases the flight control algorithms by avoiding cross-coupling effects between pitch and roll.

In this paper, we will present the results obtained in wind tunnel tests on the drone equipped with only the first control stage : the stator.

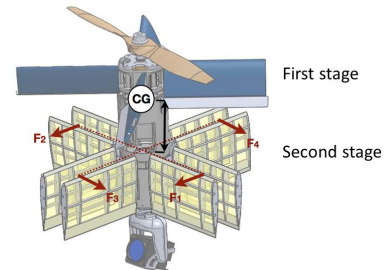


FIGURE 2 – The two control stages of the MAV of ULB

1.1 The UAV Market[3]

After a big jump in orders for military UAVs in the last decade, reports claim that the UAV market for civil unmanned aircraft will grow to \$355 million in 2020, compared to \$65 million in 2011, according to the Teal market Group. With an increasing market and reduction in federal deficit, the FAA will be under major pressure to develop rules for safely integrating UAVs into the National Airspace System.

There are numerous possible civilian uses of UAVs, such as filming floodwaters of the Red River, monitoring forest fires in Alaska and fighting whaling in Australia. There is still work to be done to regulate the use of UAVs, especially in populated areas, but "change is tough," says Mooney, noting that 20 years ago people were naysayers about GPS, which has revolutionized personal navigation.

2 GENERAL LAYOUT

2.1 Flight prototype

Figure 3 shows a cutaway view of the MAV unveiling its major components. The rotor is mounted on a permanent magnet brushless motor fixed in a solid ABS¹ housing made via rapid prototyping. On this block, the flight control systems and payload are mounted, as well as a protective shell forming the center fuselage and duct suspension rods. Each rod is bolted to an ABS housing, clamped between two carbon fiber rings. These rings ensure structural rigidity while allowing sufficient space to install the Lithium-Polymer (LiPo)

¹Acrylonitrile Butadiene Styrene is a commonly used plastic

batteries. A carbon fiber skirt forms the duct and is fixed on plastic ribs having the required duct aerodynamic profile. Note that actually most components are off-the-shelf in order to reduce cost and development time.

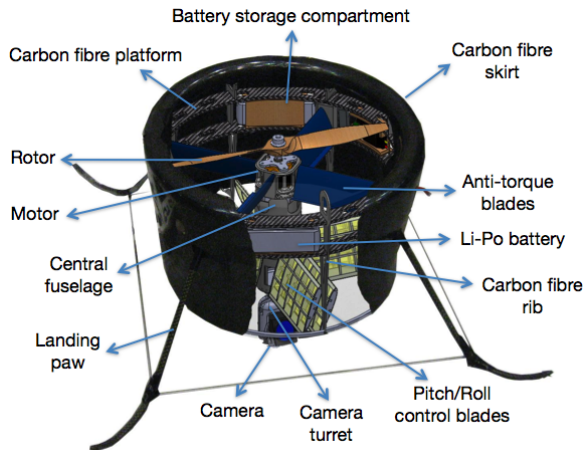


FIGURE 3 – A cutaway view of the MAV

After the first version of the ULB-designed MAV was built, the first flight tests took place. The first controlled flight of the MAV took place on May 8, 2009.

Initially, a single off-the-shelf gyroscope for yaw control was used. Tests have shown that the control vanes were effective enough to allow the UAV to move in the horizontal plane. Moreover, it was impossible to control the UAV with high level orders, as had the tendency to tip over before the pilot could react. However, the yaw control works perfectly, which validates the effectiveness of the stator with variable camber.

Two identical off-the-shelf gyroscopes have been added in the center fuselage in order to stabilize the UAV on its three axes. After this modification, the UAV could take off and reach a height of 3-4 meters. Nevertheless, it was still very difficult to control it in this configuration during flight because the gyroscopes operate in open loop. In order to improve the stability of the UAV and guide it by high level orders via radio control, a control loop should be added to each gyroscope.



FIGURE 4 – Wind tunnel test prototype

2.2 Wind tunnel test prototype

The prototype of the UAV used for wind tunnel tests (Figure 4) is currently equipped for the first test phase on the first control stage (the anti-torque stage). For these tests, four blades with non-variable camber can be set at different angles of incidence (0 to 25 degrees in increments of 5 degrees relative to the axis of rotation of the rotor). The aim is to study the effect of the angle of incidence on the anti-torque couple and on the airflow through the duct.

In an earlier numerical study, the effect of the rotor on the flow of induced air was estimated. It was concluded after analyzing the numerical results that the optimal incidence angle for the stator vanes was 7 degrees. However, numerical models for such applications are very unreliable and it is necessary to support their predictions by experimental tests.

The behavior of the airflow inside the duct is also of interest. Therefore the stator blades in the future will be equipped with pitot tubes placed throughout several sections of the four blades.

The propulsion chain (Figure 5) is composed of a brushless motor and its controller. It is supplied by two 12V car battery connected in series to deliver the necessary 24V to provide sufficient power to rotate the rotor at useful speeds. The rotation speed is controlled by a radio control system.

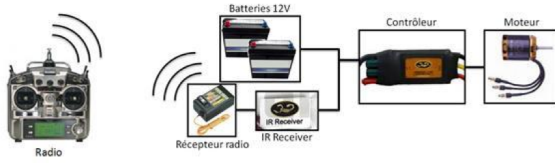


FIGURE 5 – The propulsion chain

3 WIND TUNNEL TESTING

3.1 Test plan

The tests were carried out in the University of Liège 1.5m x 2m low speed wind tunnel for various angles of attack, rotor rotational speeds and airspeeds.

The vertical axis of symmetry of the MAV was placed in the horizontal plane and mounted on an arm. One obtained a variation of the MAV angle of attack α by rotating the arm around its vertical axis (Figure 6). The rotor rotational speed was set manually via a radio transmitter and recorded optically. The anti-torque blades were fixed at 5° angle of incidence. No control blades were installed.

The tests that are being presented here was performed for an angle of attack (α) range from 0° to 10° and from 80° to 90° in steps of 5° , with a varying airspeed of the airflow far upstream the rotorcraft (V_∞) of 0, 5, 10 and 15 m/s and only one rotor rotational speed (Ω_r), i.e. 5000 RPM because too much vibrations appear above this speed (Table 1). We will discuss about the vibrations in detail in the section 3.3.1.

Test number	$V_\infty [\frac{m}{s}]$	$\alpha [^\circ]$
1	0	0
2	10	0
3	15	0
4	10	5
5	15	5
6	10	10
7	15	10
8	5	80
9	10	80
10	5	85
11	10	85
12	5	90
13	10	90

TABLE 1 – Test plan

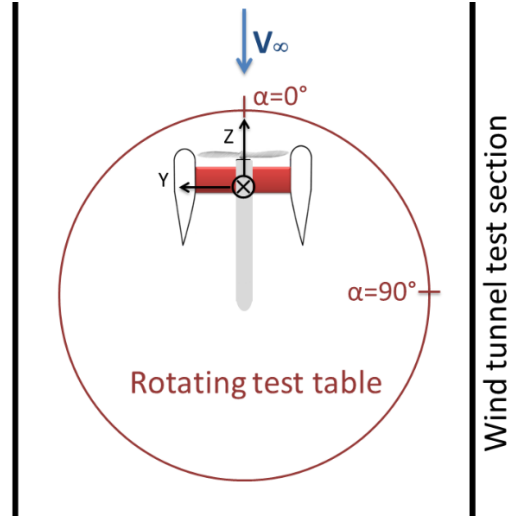


FIGURE 6 – Schematic of wind tunnel prototype mounted on rotating test table. Prototype is shown oriented at a angle of incidence α of 0° .

The test conditions were chosen to simulate hover and forward flight (Figure 7). The reader can easily see that the $\alpha=0^\circ$ to 10° positions correspond to hover and the $\alpha=80^\circ$ to 90° positions correspond to forward flight [6].

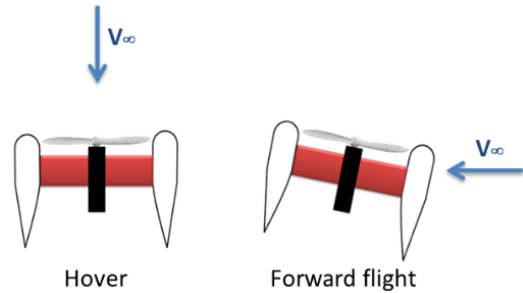


FIGURE 7 – Hover and forward flight

In the following sections, we will analyze the data collected during the tests. The natural frequencies were determined in order to establish the vibrations origin. The validity of the data was checked by means of comparisons between the results of similar tests. The reproducibility analysis is presented in the next section. After demonstrating the validity of results, we will plot the curves of dimensionless coefficients of lift, drag and pitch, and draw conclusions on the aerodynamic behavior of our model (Figure 8).

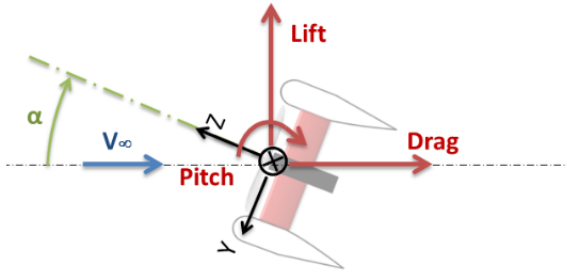


FIGURE 8 – Definitions of the coordinate systems used

3.2 Data acquisition

The instrumentation consisted of three devices. The first device was a Nano 25 six-component load sensor by ATI industrial automation. This sensor measured the forces and moments acting on the UAV. The second device was a Siemens laser tachometer, able to measure rotational speeds of up to 30.000 RPM. The third device was a Digital Power Recorder (DPR) used to record the power consumed by the brushless motor.

The test procedure is done in the following order according to Table 1 :

1. We set the angle of incidence of the drone,
2. We set the wind speed,
3. We set the rotational speed,
4. We take the measurements of forces and moments.

3.3 Data processing

3.3.1 Analysis of modes of vibration

Strong vibrations were observed during tests around 6500 RPM. The natural frequencies of the system were therefore analyzed in order to determine which mode caused the problem.

The modal analysis of the wind tunnel test prototype was carried out by means of impulsive excitation[7]. Approximate impulses were applied to the structure and the free responses were recorded.

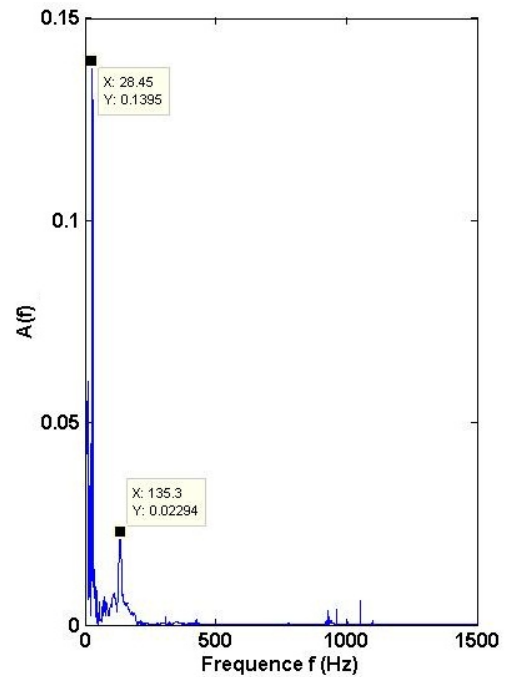
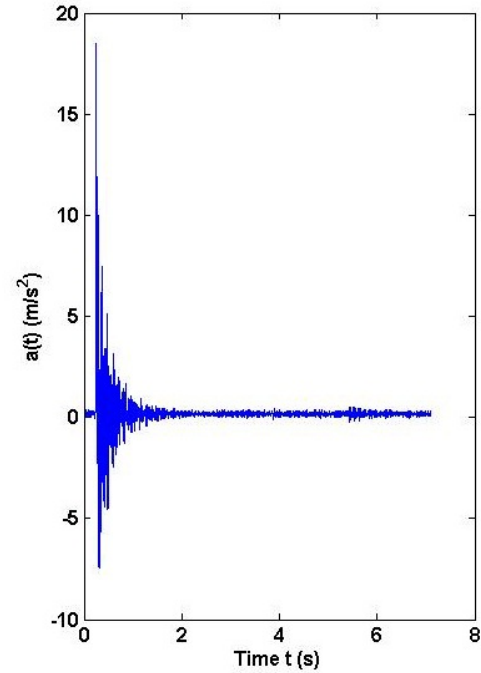


FIGURE 9 – Impulsive excitation response (top) of the wind tunnel test prototype and its spectral decomposition (bottom)

Measurement of acceleration in $\frac{m}{s^2}$ is carried out using the measure of the force along the x axis F_x (Figure 8) with the force sensor (the force is proportional to the acceleration).

3.3.2 Analysis of the noise

To be usable measurement is transformed into modal analysis by Fourier Transformer (FFT - Fast Fourier Transformation). This transforms the recorded curve "acceleration versus time" (temporary spectrum) to a curve "acceleration versus frequency" (frequency spectrum) for finding the natural frequencies.

We clearly see on the spectral decomposition (Figure 9) of the impulse responses the presence of natural frequencies with peaks at 28 Hz (1680 RPM), 112(6720 RPM) (Figure 10) and 135 Hz (8100 RPM). We have in fact observed during the tests high vibrations when the speed of rotation of the rotor reached around 6500 RPM belonging to the natural frequencies of the prototype.

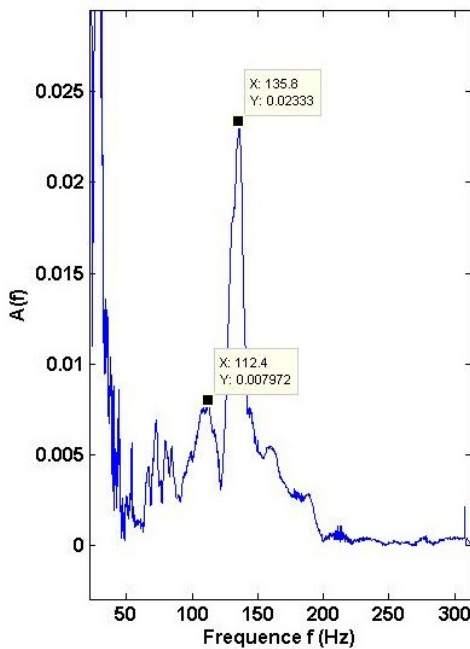


FIGURE 10 – Zoom in on the spectral decomposition around 6500 RPM (108 Hz)

It is essential for future tests to move this natural frequencies outside the range of frequencies used by the rotor. Given that the rotor can rotate at 8000 RPM, it is essential to ensure that there is no natural frequency below 133 Hz.

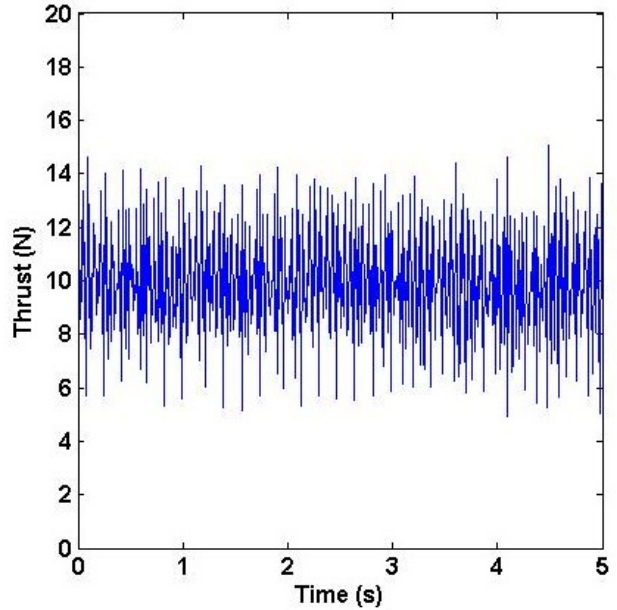


FIGURE 11 – Temporal measurement of thrust for $V_{\infty} = 10m/s$, $\alpha = 0^{\circ}$ and $\Omega_r = 5000RPM$ (raw data)

The noise content of the raw data was also assessed. Figures 12 and 13 plot the power spectral density and auto-correlation of the thrust raw data of figure 11. The sampling frequency was 100 Hz and 500 samples were recorded for each measurement. It can be seen that the noise is white in the selected frequency range. As long as the signal-to-noise ratio is acceptable, this type of noise is not problematic.

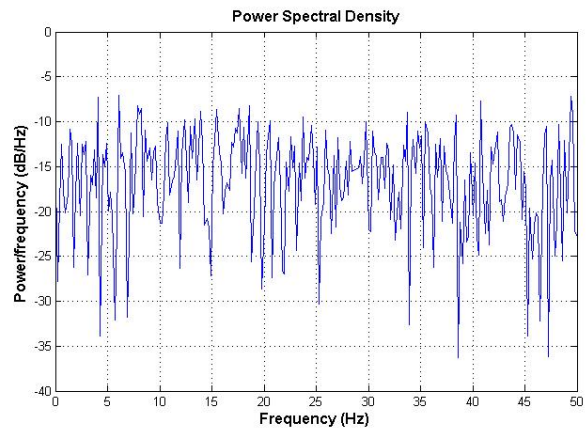


FIGURE 12 – Power density of the noise

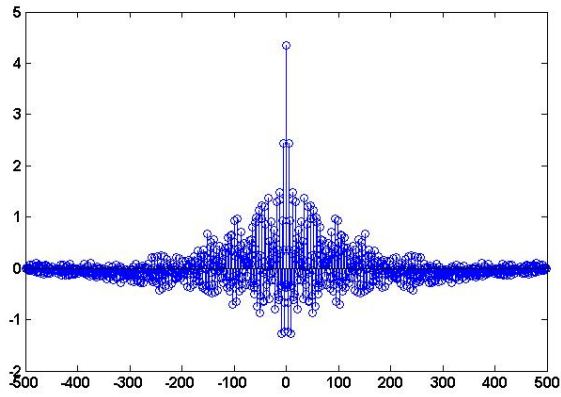


FIGURE 13 – Autocorrelation of the noise

3.3.3 Analysis of the reproducibility of the tests

In order to test the reproducibility of the tests, the test plan (Table 1) was repeated 2 times under the same conditions and the results were compared.

The averages values of the forces and moments recorded during the 13 tests of the plan (Table 1) are plotted in Figures 14 and 15. We note that the measurements are similar.

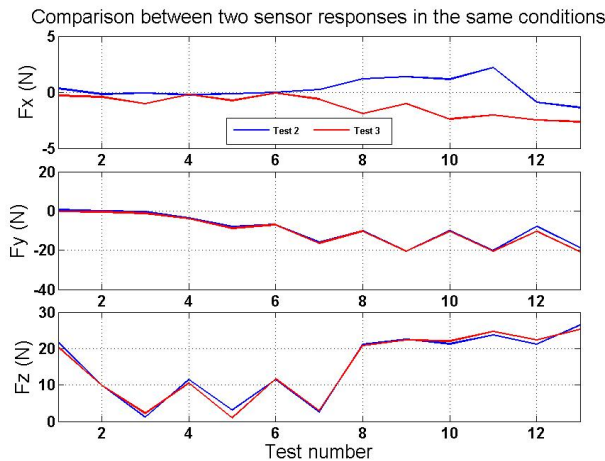


FIGURE 14 – Variation of the mean values of the three forces acting on the UAV with test number

We also see a large variation between measurements for the force F_x and the moment M_y . These variations seem significant and their sources could not be accurately determined with current data. Therefore, we will

reject these results for the data analysis.

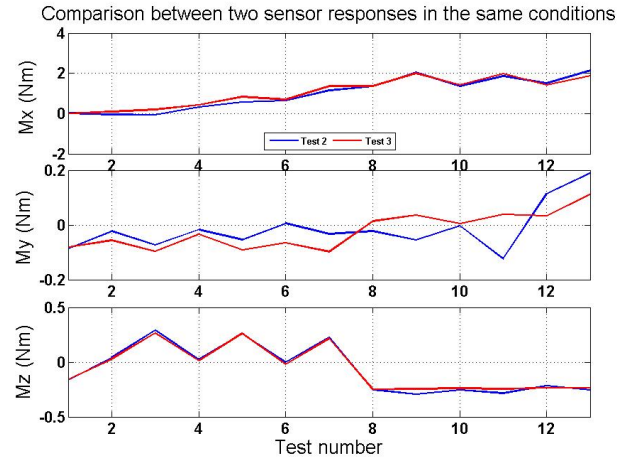


FIGURE 15 – Variation of the mean values of the three moments acting on the UAV with test number

3.4 Data analysis

Therefore we validate our results, we can calculate the aerodynamic coefficients from the forces and torques obtained during tests. According to [8], we will define the reference surface as follows :

$$S = \pi D_d \bar{c}$$

Where S =planform area
 D_d =inner-diameter of duct
 \bar{c} =duct airfoil chord

The Figure 16 represent the lift coefficient. We know from a previous study on the duct and according to a NASA study that the duct acts as a wing of infinite span ?? . You can see on the Figure 16 that the lift coefficient depends significantly on the Reynolds number. The zero lift angle is zero this is due to the symmetry of the prototype.

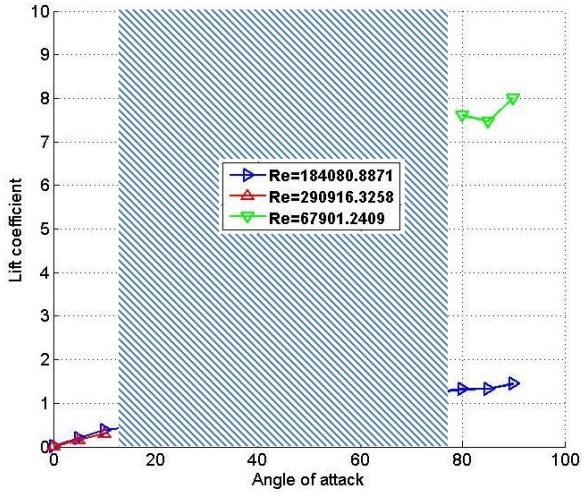


FIGURE 16 – Lift coefficient

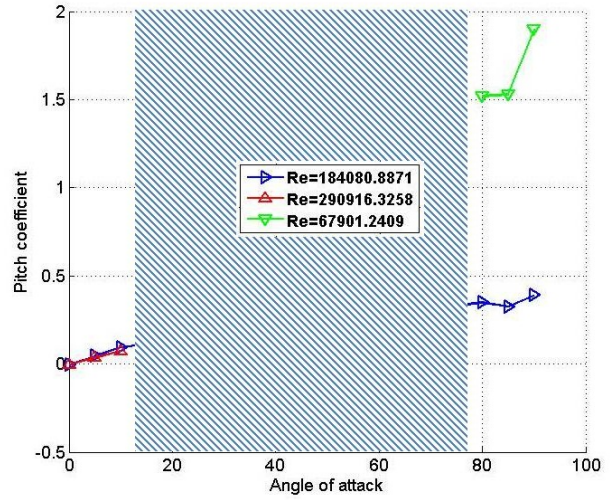


FIGURE 18 – Pitch coefficient

The beneficial effect of the duct under crosswind conditions is clear on the Figures 14. In fact, there is a level in the Fz (the thrust) measures taken for angle varying from 80 to 90 degrees with wind speed varying from 5 to 10 $\frac{m}{s}$ (tests 8-13). So the rotor is correctly protected from the bad effect of the side wind.

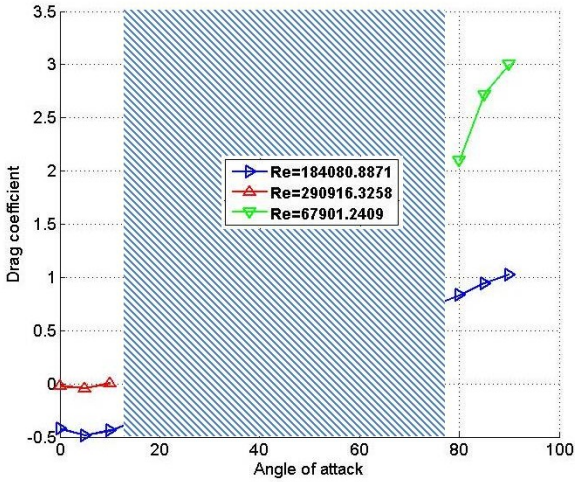


FIGURE 17 – Drag coefficient

On the Figure17 and 18 one can see that the drag and the pitch coefficients decrease significantly with the Reynolds number for forward flight ($\alpha = 80^\circ$ to 90°).

²Proton exchange membrane fuel cells

4 PROPULSION SYSTEM

In order to maximise the MAV's autonomy, fuel cells (FC) are being considered as a viable energy source. The process of integrating fuels cells onto the MAV has been started.

Therefore, an important part of the MAV is the small hydrogen tank needed for the PEMFC². In this section of the paper, the design study for this gaseous hydrogen storage tank is described.

The first step in the design process is to determine the H_2 flow rate of the fuel cell. First, the computational method used to estimate the mass flow of hydrogen as a function of power consumption will be presented. Subsequently, the required volume of the hydrogen tank will be determined.

4.1 Faraday's method for fuel flow computation

The fuel flow consumption can be written as a function of the current, i.e. [2] :

$$N_{H_2} = \frac{I}{2F}$$

Where N_{H_2} is the hydrogen flow rate in g/s, F is the Faraday constant ($F = 96485 \frac{C}{mol}$) and I the current in ampere.

This expression gives the fuel consumption of a single fuel cell. For multiple fuel cells, the flow rate

must be multiplied by the number of fuel cells. The calculation yields the minimum fuel cell consumption. In reality, the flow rate required must be more important because there are hydrogen losses. The phenomenon of reverse current through the membrane is also neglected.

4.2 Experimental method

To have a good idea of fuel flow in function of different power supply, we can obtain an experimental curve speaking about the relation between power supply and hydrogen flow rate. Here you can see a curve obtained for the Aeropak system proposed by Horizon Energy Systems. [10] obtain this experimental curve for a power supply by a fuel cell for the power interval 0-200. Above 200 W, the rest of power is provided by Li-Po batteries with an hybrid system.

A possibility to know the mass hydrogen consumed is to test different flight phase and take some measure of the power consumption. After that, we can expose different hydrogen flow rate in function of different phases to design the hydrogen mass consumption for a particular flight. We are now able to determine the volume of our hydrogen gas tank.

4.3 Gaseous hydrogen tank

A possibility to know the mass hydrogen consumed is to test different flight phases and take some measurements of the power consumption. After that, we can expose different hydrogen flow rates in function of different flight phases to design the hydrogen mass consumption for a particular flight profile. We are now able to determine the volume of our hydrogen gas tank.

$$P = \rho \frac{RT}{M}$$

Where :

$$\begin{aligned} R &= 8,314 JK^{-1} mol^{-1}, \\ T &= \text{ambient temperature}, \\ M &= \text{molar mass, } m = \text{mass of } H_2 \\ \rho &= \text{density} = \frac{m}{V}. \end{aligned}$$

Therefore,

$$V = \frac{mRT}{PM}.$$

The pressure P(Pa) depends on the technology available for gaseous hydrogen storage. For more information, you can read the article "Development of high pressure gaseous hydrogen storage technologies"[11]. The maximum pressure obtained nowadays is 700 bars

with tanks based carbon fiber materials. The last variable to determine is the requested volume of our hydrogen tank (V).

5 CONCLUSIONS AND PROSPECTS

Several tests have already been conducted on the drone. We have noticed a lot things to take into account in future trials and to improve the prototype.

We found it is important to have good fasteners to avoid that they be unscrewed during tests. The model currently used for the wind tunnel is the first model built for this UAV wind tunnel test. It is therefore under constant improvement. The wind tunnel test procedure is also being adjusted to ensure the best possible data quality.

Also, some problems of power and rotation speeds recording have been observed. DPR used is not stable and the data acquisition program provided with this equipment often crashes. Concerning the laser type tachometer, this measurement system for the rotation speed requires the presence of an additional person. For the new version of the prototype, it would be interesting to design a new acquisition system that would record the power and rotation speed and would control the speed via the human machine interface. To do so, we will place the tachometer inside the duct and connect it directly to the interface. Radio control will be removed and the control command will be given directly through the interface.

It is essential for future tests to move the natural modes outside the range of frequencies used by the rotor. Given that our rotor can rotate at 8000 RPM, it is essential to ensure that there is no natural mode below 133 Hz. For this, we will build a new mounting arm to eliminate this phenomenon.

A first study was also done to design the volume of the hydrogen gaseous storage for a fuel cell propulsion system. In another study, we can test the validity of our computation methods. It is also important to take into account the hydrogen tank weight in the UAV design. A detailed study of risk must be done because the hydrogen is a very flammable. Several tanks with different pressure storage system must be tested to determine what is the recommended choice for our application.

6 Acknowledgements

The authors would like to recognize and thank Professor Greg Dimitriadis and Thomas Adrienne for their guidance and assistance during the wind tunnel tests and the writing of this paper.

Références

- [1] Igor Astrov and Andrus Pedai. Motion control of tuav having eight rotors for enhanced situational awareness. *World Academy of Science, Engineering and Technology*, 60, 2011.
- [2] Virginie Delcour. *Implémentation et validation expérimentale d'un modèle de PEMFC*. PhD thesis, Université Libre de Bruxelles, may 2008.
- [3] Jen Dimascio. Industry cautious about growth for civilian uavs in u.s. market. *Aviation Week & Space Technology*, pages 66–67, 2012.
- [4] Dae-Yeon Won Dong-Wan Yoo and Min-Jea Tahk. Optical flow based collision avoidance of multi-rotor uavs in urban environments. *International Journal of Aeronautical & Space Science*, 12(3) :252–259, 2011.
- [5] Dae-Yeon Won Dong-Wan Yoo, Hyon-Dong Oh and Min-Jea Tahk. Dynamic modeling and stabilization techniques for tri-rotor unmanned aerial vehicles. *International Journal of Aeronautical & Space Science*, 11(3) :167–174, 2010.
- [6] K. J. Goodson, K. W.; Grunwald. Division of aerodynamic loads on a semispan tiltingducted-propeller model in hovering and transition flight. *Langley Research Center*, mois May 1, 1962.
- [7] Broch J.T. *Mechanical vibration and shock measurements*. Bruel&Kjaer. 2nd Edition, 1984.
- [8] Martin Preston and Tung Chee. Performance and flowfield measurements on a 10-inch ducted rotor vtol uav. *Technical report*, 2004. NASA.
- [9] Roland Siegwart Samir Bouabdallah, Pierpaolo Murrieri. Design and control of an indoor micro quadrotor. Autonomous Systems Laboratory Swiss Federal Institute of Technology Lausanne, Switzerland.
- [10] Jennifer L. PALMER. VERSTAETE Dries, James R. HARVEY. Hardware-in-the-loop simulation of fuel-cell-based hybrid-electrical uav propulsion. *28TH International Congress of the Aeronautical Sciences*, 2012.
- [11] Ping XU Pengfei LIU Yonghi ZHAO Jian YANG. ZHENG Jinyang, Xianxin Liu. Development of high pressure gaseous hydrogen storage technologies. *International Journal of Hydrogen energy*, 2011.